Evidence for Oxidation-State-Dependent Conformational Changes in Human Ferredoxin from Multinuclear, Multidimensional NMR Spectroscopy[†,‡]

Bin Xia,[§,||,⊥] Brian F. Volkman,[||] and John L. Markley*[,§,||]

Graduate Program in Biophysics and Department of Biochemistry, University of Wisconsin−Madison, 420 Henry Mall, Madison, Wisconsin 53706

Received November 3, 1997; Revised Manuscript Received December 23, 1997

ABSTRACT: Human ferredoxin belongs to the vertebrate ferredoxin family which includes bovine adrenodoxin. It is a small (13.8 kDa) acidic protein with a [2Fe-2S] cluster. It functions as an electron shuttle in the cholesterol side-chain cleavage reaction which is the first step of steroid hormone biosynthesis. The protein studied here was produced in *Escherichia coli* and doubly labeled with ^{13}C and ^{15}N. The diamagnetic ^{15}N, $^{13}C'$, $^{13}C^{\alpha}$, $^{13}C^{\beta}$, $^{1}H^{\alpha}$, and $^{1}H^{N}$ resonances from about 70% of the 124 amino acid residues for oxidized human ferredoxin and 80% of those for the reduced protein have been assigned primarily on the basis of results from three-dimensional, triple-resonance experiments. Secondary structure features for human ferredoxin in its oxidized and reduced states have been identified from a combination of chemical shift index and NOE data. Comparison of NMR results from the protein in its oxidized and reduced states indicates that structural changes accompany the change in the oxidation state of the [2Fe-2S] cluster. Major differences are localized at two regions: residues 29−31 and residues 109−124; the latter stretch forms the C-terminal region of the protein. The possible functional significance of these oxidation-state-dependent structural changes is discussed.

Human ferredoxin (HuFd), a small (13.8 kDa) acidic protein with a single [2Fe-2S] cluster, is found in the mitochondria of steroid metabolizing tissues. It was cloned first from human placental tissue (*1*). Human ferredoxin belongs to the vertebrate ferredoxin family, whose members exhibit a high degree of sequence homology (*2*). Vertebrate ferredoxins function to transfer reducing equivalents from NADPH-dependent ferredoxin oxidoreductase to cytochrome $P450_{scc}$ enzymes involved in the biogenesis of steroid hormones, the formation of vitamin D metabolites, and the production of bile acids. They have been found to be involved in the initial step of progesterone biosynthesis in which the side chain of cholesterol is cleaved to yield pregnenolone (*3, 4*).

Human ferredoxin has 124 amino acid residues with cysteines at five positions: 46, 52, 55, 92, and 95. Four of the cysteines provide the ligation of the [2Fe-2S] cluster, and the fifth cysteine, Cys^{95}, has a free −SH. In the oxidized state, both irons in the iron−sulfur cluster are high-spin Fe(III) and are antiferromagnetically coupled in the ground state ($S = 0$). Thermal population of excited states accounts for the paramagnetic effects observed in NMR spectra of oxidized HuFd at physiological temperatures. In the reduced state ($S = {}^1/_2$), one iron is Fe(III) and the other is Fe(II), and paramagnetic effects are observed at all temperatures.

No three-dimensional structure has been published for any of the vertebrate ferredoxins. Bovine adrenodoxin has been the subject of X-ray crystallographic (*5, 6*) studies for more than two decades. Conventional ^{1}H NMR spectroscopy has been utilized to study bovine adrenodoxin, but no complete sequence-specific assignments for that protein have been published (*7, 8*). A low-resolution NMR structure has been reported for putidaredoxin, a bacterial [2Fe-2S] protein functionally related to vertebrate ferredoxins (*9*). It has been assumed that the structures of vertebrate ferredoxins resemble those of putidaredoxin because of sequence and spectral similarities.

Histidine 56, which is conserved among all known vertebrate ferredoxins, was once proposed to be hydrogen-bonded to the iron−sulfur cluster and play an important role in determining the reduction potential (*10, 11*). Subsequent investigation demonstrated, however, that none of the histidines in human ferredoxin interacts directly with the cluster (*2*). We recently described a method for the efficient overexpression of human ferredoxin in *Escherichia coli* and used this approach to produce analogues with Cys-to-Ser substitutions at each of the four of the cluster ligands for spectroscopic analysis (*12*). Here, we report the sequence-specific assignments for N, C', C^{α}, C^{β}, H^{α}, and H^{N} resonances for oxidized and reduced human ferredoxin along with an analysis of the secondary structural elements. The results show

[†] This research was supported by NIH Grants GM35976 and RR02301. Spectroscopy was performed at the National Magnetic Resonance Facility at Madison which is subsidized by the Biomedical Research Technology Program, Division of Research Resources, NIH (RR02301), and the University of Wisconsin. Additional funds for equipment came from the NSF Biological Biomedical Research Technology Program (DMB-8415048), NIH Shared Instrumentation Program (RR02781), and the U.S. Department of Agriculture.

[‡] NMR data and derived structural results have been deposited at BioMagResBank under accession number 4073 (for oxidized human ferredoxin) and 4074 (for reduced human ferredoxin).

* Author to whom correspondence should be addressed.

[§] Graduate Program in Biophysics.

[||] Department of Biochemistry.

[⊥] Present address: Department of Molecular Biology, MB-2, The Scripps Research Institute, 10550 N. Torrey Pines Road, La Jolla, CA 92037.

S0006-2960(97)02722-0 CCC: $15.00
Published on Web 02/27/1998

Table 1: Spectral Parameters for the NMR Data Sets Collected on Human Ferredoxin[a]

	d_1 (^{1}H)[b]		d_2			d_3			
experiment	SF (MHz^{-1})	SW (Hz^{-1})	nucleus	SW (Hz^{-1})	N_2[c]	nucleus	SW (Hz^{-1})	N_3[c]	matrix size ($d_1 \times d_2 \times d_3$)
2D ^{1}H−^{15}N HSQC	500.13	6009.615	^{15}N	1666.67	256				512 × 256
3D HNCO	500.13	6009.615	^{13}C′	2000.00	64	^{15}N	1666.67	36	512 × 256 × 128
3D HNCA	500.13	6009.615	$^{13}C^{\alpha}$	4545.45	60	^{15}N	1666.67	32	512 × 256 × 128
3D HN(CO)CA	500.13	6009.615	$^{13}C^{\alpha}$	4545.45	64	^{15}N	1666.67	28	512 × 256 × 128
3D HNCACB	500.13	6009.615	$^{13}C^{\alpha/\beta}$	7352.94	64	^{15}N	1666.67	32	512 × 256 × 128
3D CBCA(CO)NH	500.13	6009.615	$^{13}C^{\alpha/\beta}$	7352.94	42	^{15}N	1666.67	32	512 × 256 × 128
3D HCACO	500.13	6009.615	^{13}C′	2000.00	64	$^{13}C^{\alpha}$	4545.45	32	512 × 256 × 128
3D ^{13}C-NOESY[d]	500.13	4006.41	^{1}H	4006.41	80	^{13}C	9090.91	64	512 × 512 × 128
3D ^{15}N-TOCSY[d]	750.13	8992.806	^{1}H	8992.806	128	^{15}N	2500	32	512 × 512 × 128
3D ^{15}N-NOESY[d]	750.13	8992.806	^{1}H	8992.806	128	^{15}N	2500	32	512 × 512 × 128
3D ^{13}C-NOESY[e]	750.13	6009.62	^{1}H	4166.67	128	^{13}C	9090.91	56	512 × 512 × 128
3D ^{15}N-TOCSY[e]	600.13	6944.444	^{1}H	6944.444	150	^{15}N	1818.18	40	512 × 512 × 128
3D ^{15}N-NOESY[e]	600.13	6944.444	^{1}H	6944.444	150	^{15}N	1818.18	40	512 × 512 × 128

[a] The parameters listed here apply to NMR data sets for both oxidized and reduced human ferredoxin, except for 3D ^{15}N-TOCSY, 3D ^{15}N−NOESY, and 3D ^{13}C−NOESY data. [b] A total of 1024 complex points were collected in the ^{1}H dimension (d_1) of all experiments. In all experiments except the HCACO, the right half of the spectrum (upfield of H_2O) in d_1 dimension contained no signals and was discarded. [c] N_2 and N_3 are the numbers of complex points collected for d_2 and d_3 dimensions, respectively. [d] NMR experimental data collected for oxidized HuFd. [e] NMR experimental data collected for reduced HuFd.

that changes in secondary structure and local mobility accompany the change in oxidation state. The secondary structure of human ferredoxin in both its oxidation states was found to differ in certain regions from that reported for oxidized putidaredoxin.

MATERIALS AND METHODS

Chemicals and E. coli Strains. $^{15}NH_4Cl$, [99% U-^{13}C]-glucose, and [98% U-^{2}H]glycerol were purchased from CIL (Cambridge Isotope Laboratories, Andover, MA). Sodium dithionite (assay > 87%) was purchased from Fluka Chemical Corp. (Ronkonkoma, NY). *E. coli* strain BL21(DE3)/pLysS was purchased from Novagen (Madison, WI).

Protein Expression and Purification. Human ferredoxin was produced in *E. coli* by using the T7 bacteriophage RNA polymerase/promoter expression system (*12*). The cDNA encoding human ferredoxin (*1*, *13*) was cloned into expression vector pET9a to yield a new plasmid HuFd/pET9a. This new plasmid was transformed into *E. coli* strain BL21/pLysS for protein production.

The cells were lysed by a freeze−thaw cycle followed by sonication. The protein was purified first by in vitro reconstitution (*13*), and the reconstituted ferredoxin was purified further by ion-exchange chromatography and gel filtration. Protein fractions with $OD_{414}/OD_{276} > 0.78$ were considered pure and used for further study. A complete description of overexpression and protein purification is given elsewhere (*12*).

Preparation of Labeled Protein Samples. Uniformly ^{15}N-labeled and ^{15}N, ^{13}C doubly labeled HuFd were prepared as follows. One bacterial colony of *E. coli* strain BL21/pLysS with plasmid HuFd/pET9a was grown in 5 mL of LB medium with 100 mg/L kanamycin and 34 mg/L chloramphenicol for 10 h. This cell culture (100 μL) was used to inoculate 100 mL of M9 medium with labeled compounds. Each liter of this medium contained 6 g of Na_2HPO_4, 3 g of KH_2PO_4, 0.5 g of NaCl, 0.25 g of $MgSO_4 \cdot 7H_2O$, and 0.050 g of thiamine. For uniform ^{15}N labeling, 5 g of glucose and 1 g of 99.8% $^{15}NH_4Cl$ were used in the M9 medium; for double labeling, 2 g of [99% U-^{13}C]glucose and 1 g of 99.8% $^{15}NH_4Cl$ were used. Antibiotics kanamycin (100 mg/L) and chloramphenicol (34 mg/L) were added to the medium. After overnight incubation in a shaker at 37 °C, this 100 mL culture was transferred into a 2.8 L flask containing 900 mL of the same labeled M9 medium. The culture was incubated at 37 °C with shaking until the OD_{600} reached 0.7. IPTG (100 mg) was added to induce the expression of T7 RNA polymerase. After 16 h of continuous incubation in a 37 °C shaker, the bacteria were harvested by centrifugation.

NMR Sample Preparation. About 10 mg of HuFd was used for each NMR sample with concentrations around 1.5 mM. Protein concentrations were determined by using $\epsilon_{414} = 11\ mM^{-1}\ cm^{-1}$ (*14*). Amicon stirred cells and YM10 and YM3 membranes were used to concentrate the protein and to exchange the buffer. Oxidized NMR samples were in 50 mM Tris·HCl buffer (pH 7.2) containing 50 mM NaCl and 5% [U-^{2}H]glycerol in 90% ^1H_2O and 10% ^2H_2O.

The reduced HuFd sample was in 50 mM phosphate buffer (pH 7.4) containing 50 mM NaCl in 90% ^1H_2O and 10% ^2H_2O. To reduce human ferredoxin, each protein sample was first deaerated by vacuum; then the sample was transferred into a 5 mm NMR tube containing 1.5 mg sodium dithionite. After further degassing, the NMR tube was sealed by flame under vacuum. The pH value was not measured after reducing the protein. It is estimated that the added dithionite decreased the pH of the reduced HuFd solution to about pH 7.2.

NMR Spectroscopy and Data Processing. Table 1 contains a complete list of the experiments performed on HuFd, including the spectral parameters. NMR data sets were collected at 10 °C on Bruker DMX-500, DMX-600, and DMX-750 spectrometers (Bruker Instruments, Inc., Billerica, MA). Both spectrometers were equipped with Bruker ^{1}H, ^{13}C, ^{15}N triple-resonance probe heads with three-axis self-shielded gradient coils. Spectra were acquired with Xwin-NMR software, v1.1 (Bruker). Previously described data collection methods were used (*15*, *16*) with minor changes: magic angle (instead of *Z*-) gradients were employed for coherence selection and sensitivity enhancement, which resulted in improved suppression of the water solvent signal; the water

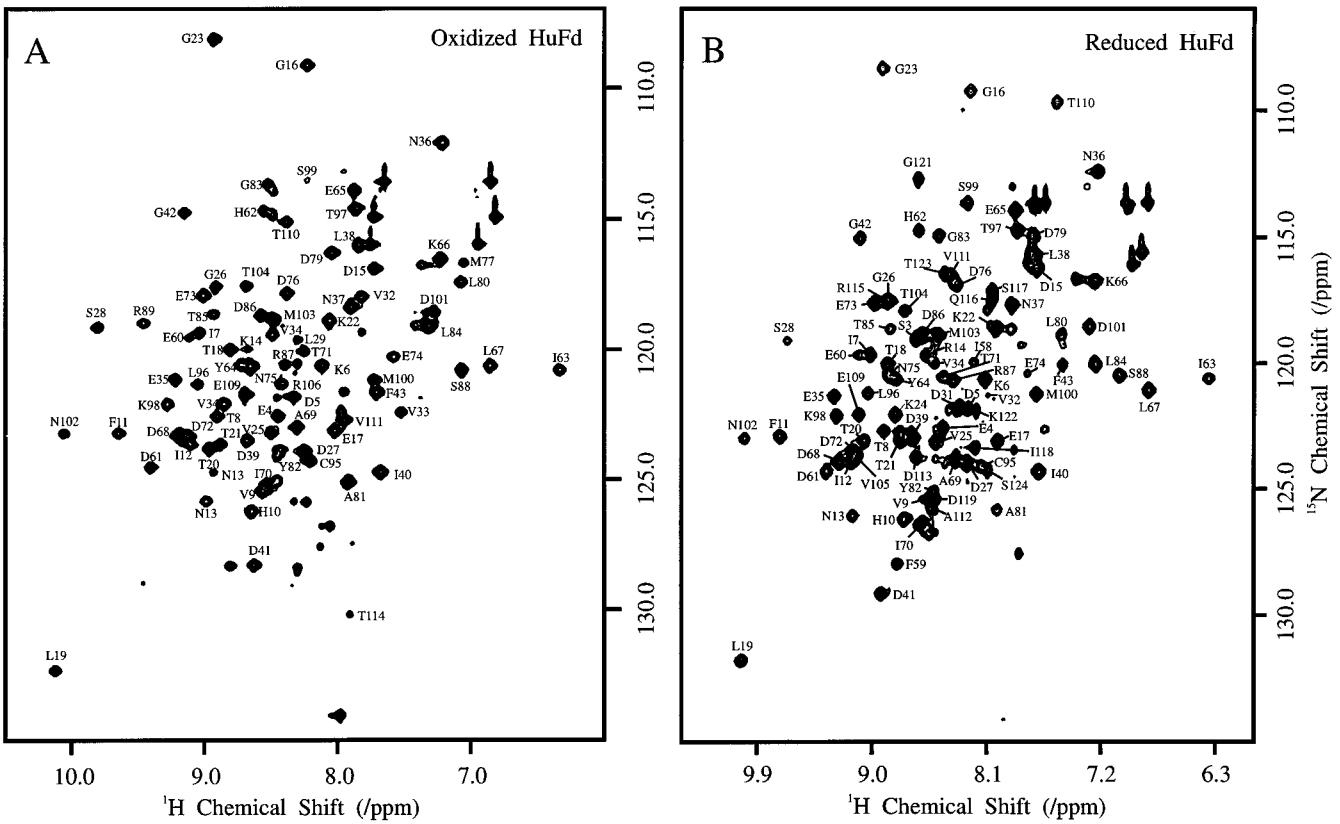

FIGURE 1: 2D ^{1}H[^{15}N] HSQC spectrum of a sample of oxidized and reduced [U-^{15}N, ^{13}C]human ferredoxin, at 10 °C. Assignments for cross-peaks are indicated by the one-letter amino acid code and residue number.

signal was minimally saturated in all experiments except HCACO and CBCA(CO)NH. Triple-resonance experiments were optimized by using continuous ^{1}H decoupling (*16*).

The sample of oxidized [U-^{15}N]HuFd used for the hydrogen exchange study was first exchanged with 50 mM Tris·HCl buffer (pH 7.2) containing 50 mM NaCl and 5% [U-^{2}H]-glycerol in $^{1}H_2O$. It was then lyophilized and redissolved in $^{2}H_2O$. 2D ^{1}H[^{15}N] HSQC-SE data were collected every 30 min for 20 h on this sample.

NMR data were processed on Silicon Graphics workstations with FELIX software (version 2.30 or 95.0*β*; Molecular Simulations, Inc., San Diego, CA). ^{1}H chemical shifts were measured relative to internal DSS (taken as 0 ppm). The ^{15}N and ^{13}C chemical shifts were referenced indirectly to DSS by multiplying the spectrometer frequency corresponding to 0 ppm in the ^{1}H spectrum by the ^{15}N/^{1}H frequency ratio or by the ^{13}C/^{1}H frequency ratio reported by Wishart et al. (*17*). Corrections were made for the effect of temperature on the chemical shift reference (*18*).

Software packages used in NMR data analysis and assignments included PEAKPICK for picking all peaks (*19*) and CONTRAST for semi-automated assignments (*20*, *21*). The computer program CSI (*22*) was used for determining the chemical shift index.

RESULTS

Assignment Strategy. Sequential assignments of the diamagnetic NMR signals of ^{15}N and ^{13}C doubly labeled human ferredoxin samples in $^{1}H_2O$ were based solely on data from a series of 3D triple-resonance experiments: HNCO, HNCA, HN(CO)CA, HNCACB, and CBCA(CO)NH. Each experiment provided particular atom correlations: $H^N(i)$-N(i)-$C^\alpha(i)$ from HNCA, $H^N(i)$-N(i)-$C^\alpha(i-1)$ from HN(CO)CA, $H^N(i)$-N(i)-$C^\alpha(i)$ and $H^N(i)$-N(i)-$C^\beta(i)$ from HNCACB, and $C^\alpha(i-1)$-N(i)-$H^N(i)$ and $C^\beta(i-1)$-N(i)-$H^N(i)$ from CBCA(CO)NH. The ^{1}H[^{15}N] HSQC-SE experiment provided the reference spectrum to which individual cross-peaks from the 3D triple resonance experiments were related. ^{1}H−^{15}N correlation peaks (except those from side chains) are unique for individual amino residues. HNCO data were used to resolve overlapped peaks in the HSQC spectra. Thus, $^{13}C^\alpha$ and $^{13}C^\beta$ chemical shifts for a given residue (associated with a ^{1}H−^{15}N correlation peak) and the previous residue in the sequence were determined from HNCA, HN(CO)CA, HNCACB, and CBCA(CO)NH experiments. Sequential connections were then extended by matching intra-residue and inter-residue $^{13}C^\alpha$ and $^{13}C^\beta$ chemical shifts. Signals from certain amino acid types, such as threonine, alanine, and glycine, were recognized easily from their unique $^{13}C^\alpha$ and $^{13}C^\beta$ chemical shifts values. This information provided starting points for sequence-specific assignments. Assignments made in this way were confirmed later with sequential $^{1}H^\alpha$ chemical shift information from 3D ^{1}H[^{15}N] TOCSY−HSQC and HCACO experiments.

Backbone Sequential Assignments. Figure 1 shows the 2D ^{1}H[^{15}N] HSQC spectrum of oxidized and reduced HuFd with assignments indicated. For oxidized HuFd, sequence-specific assignments were determined for about 70% of the 124 amino acid residues. Most of the unassigned residues are located in three regions: residues 42−57, residues 90−94, and residues 115−124. In addition, residues 30, 107, and 108 were not assigned. The first two regions are near the ligand cysteines, which have been shown to be affected by the paramagnetism of the [2Fe-2S] cluster (B. Xia and J.

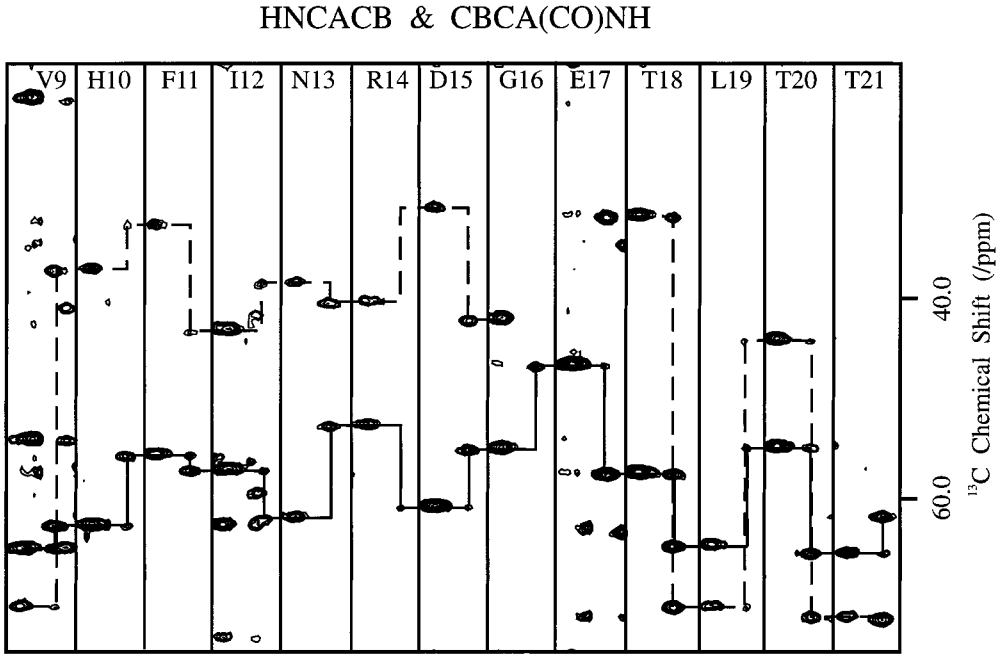

FIGURE 2: Strip plot of HNCACB and CBCA(CO)NH data that show the sequential connections for the resonances from $^{13}C^{\alpha}_{i}$ (solid lines) and $^{13}C^{\beta}_{i}$ (broken lines) nuclei of residues 9−21 of oxidized human ferredoxin. In each strip, HNCACB data are on the right side, and CBCA(CO)NH data are on the left.

L. Markley, unpublished results). The dynamic properties of the C-terminal region discussed below may be responsible for the absence of signals from residues 115−124 in the data sets.

About 80% of the total 124 residues were assigned for reduced HuFd. Signals from the last 10 residues, missing in spectra of the oxidized protein, were identified in NMR spectra of reduced HuFd. The two major unassigned regions were similar to those of the oxidized protein: residues 44−57 and 90−94. In addition, residues 29, 77, 78, 106−108, and 114 were not assigned. $^{1}H^{\alpha}$ and $^{13}C^{\beta}$ chemical shifts for a few assigned residues were not identified due to the lack of corresponding peaks in NMR spectra.

Figure 2 shows representative sequential assignments determined from HNCACB and CBCA(CO)NH data. In each strip, HNCACB data are on the right and CBCA(CO)-NH data are on the left. Sequential connections for $^{13}C^{\alpha}$ are indicated by solid lines, and those for $^{13}C^{\beta}$ are indicated by broken lines. Signals from the unique Thr-Thr dipeptide in HuFd were identified easily from the characteristic $^{13}C^{\alpha}$ and $^{13}C^{\beta}$ chemical shifts, and this determined the alignment of these sequential assignments with the protein sequence.

Secondary Structure from Chemical Shift Index. The multinuclear chemical shift index (CSI) (*23*) was determined from the $^{1}H^{\alpha}$, $^{13}C'$, $^{13}C^{\alpha}$, and $^{13}C^{\beta}$ chemical shifts of oxidized and reduced HuFd. The results for oxidized HuFd (Figure 3, top) indicated the presence of four helices (residues 31−35, 61−64, 72−79, and 98−102) and three β-strands (residues 6−12, 18−24, and 104−106).

The results for reduced HuFd (Figure 3, bottom) indicate the presence of three helices and three β-strands. The first helix predicted for oxidized HuFd is not indicated by the consensus CSI plot for the reduced protein. The other three helices are located at the same positions as those in the oxidized protein. The first two strands indicated for reduced

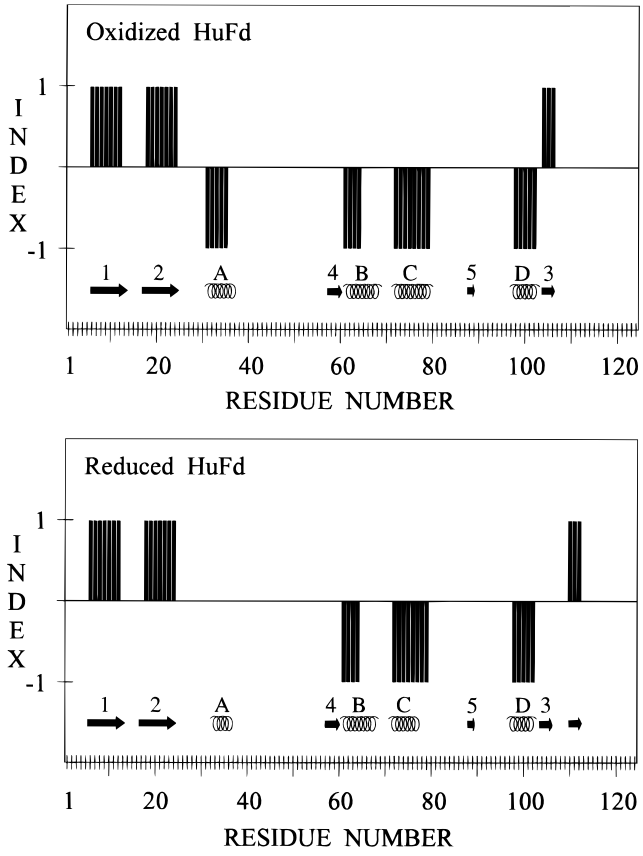

FIGURE 3: Consensus chemical shift index from $^{1}H^{\alpha}$, $^{13}C^{\alpha}$, $^{13}C^{\beta}$, and $^{13}C'$ for human ferredoxin: (top) oxidized state, (bottom) reduced state. Secondary structure features derived from NOE data are indicated.

HuFd are identical to those predicted for the oxidized protein, but the last strand is displaced by six residues (110−112).

Secondary Structure from NOE Data. Data from the 3D $^{1}H[^{15}N]$ NOESY−HSQC spectrum of oxidized HuFd are

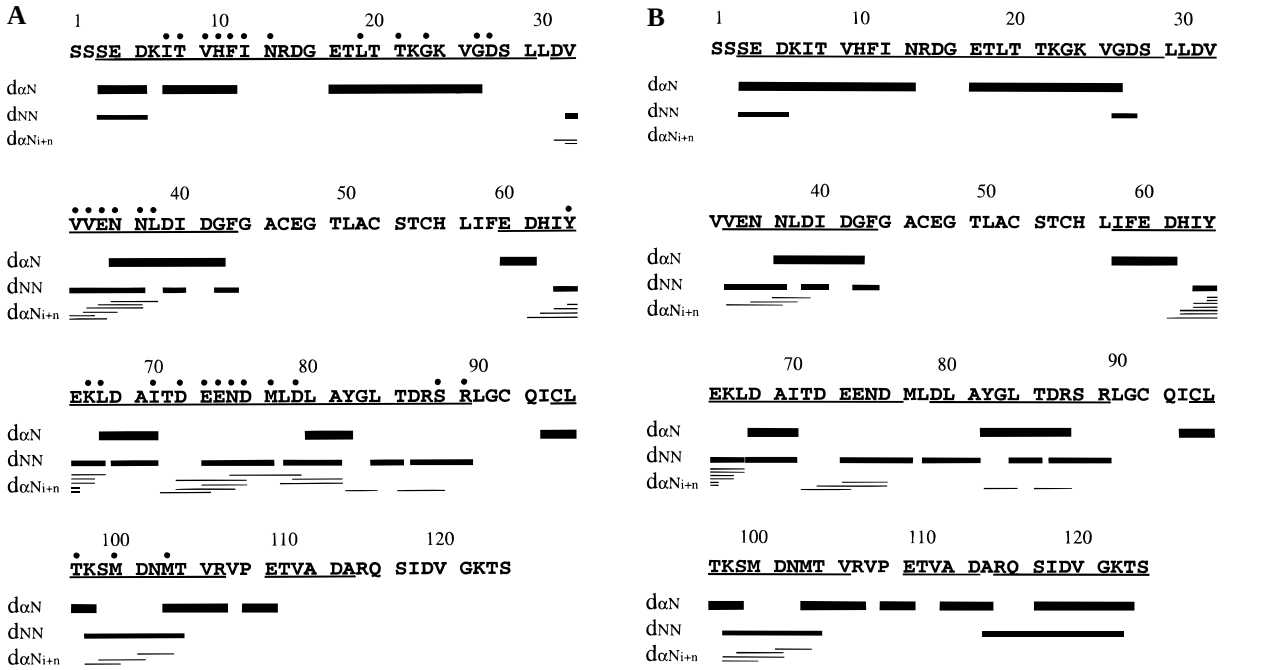

FIGURE 4: Summary of observed sequential NOE connectivities and hydrogen exchange data for (A) oxidized human ferredoxin and (B) reduced human ferredoxin. Underlined letters denote residues that were assigned; others were not assigned. The black dots above the residues indicate slowly exchanging backbone amide hydrogens (determined only for oxidized human ferredoxin), as defined by the observation of cross-peaks in the $^{1}H[^{15}N]$ HSQC spectrum taken after 15 h after solvent exchange ($^{1}H_2O$ to $^{2}H_2O$).

summarized in Figure 4A. An α-helix is characterized by distinctive patterns of short-range NOEs: $H^{\alpha}_{i}-H^{N}_{i+3}$, $H'_{i}-H^{N}_{i+1}$, $H^{\alpha}_{i}-H^{N}_{i+2}$, and $H^{\alpha}_{i}-H^{N}_{i+4}$, etc. (*24*). The presence of the four helices was confirmed by short-range sequential NOE data (Figure 4A). The NOE data show that helix A (31−37) extends to residue 37, instead of 35 as predicted by the CSI, and that helix B (61−67) extends to 67, instead of 64. Cross-strand NOEs observed in ^{15}N- and ^{13}C-edited 3D NOESY spectra indicate that the three strands identified by the CSI form a mixed β-sheet as shown in Figure 5. The first and second β-strands are antiparallel, whereas the third is parallel with the first. The NOE data supported the addition of one more residue to each strand predicted by CSI; thus the three strands consist of 6−13, 17−24, and 103−106.

Although not suggested by CSI analysis, NOEs identified in the ^{15}N-edited NOESY spectrum of oxidized HuFd are consistent with the presence of two additional strands of antiparallel β-sheet as observed by Ye and Pochapsky in the structure of oxidized putidaredoxin (*25*) (Figure 5). These NOEs are the $H^{N}-H^{N}$ NOE between Thr^{104} (in strand 3) and Glu^{60}, linking strands 3 and 4, and the $H^{N}-H^{\alpha}$ NOE between Phe^{59} and Ser^{88} H^{α}, linking strands 4 and 5.

The NOE data for reduced HuFd (Figure 4B) suggest that helix A observed in oxidized HuFd (31−37) is not missing entirely in reduced HuFd, as predicted by CSI (Figure 3B), but instead is reduced in length to 34−37. In addition, the NOE data suggest that helix C also is shorter in reduced HuFd than in the oxidized protein. In the spectra of reduced HuFd, no signals were assigned to residues 77 or 78. The first three β-strands observed in the oxidized protein appear to be retained in the reduced state (Figure 5), as indicated by cross-strand NOE data. Evidence for the presence of strands 4 and 5 is relatively weaker for the reduced protein than for the oxidized form. The residues in these stretches

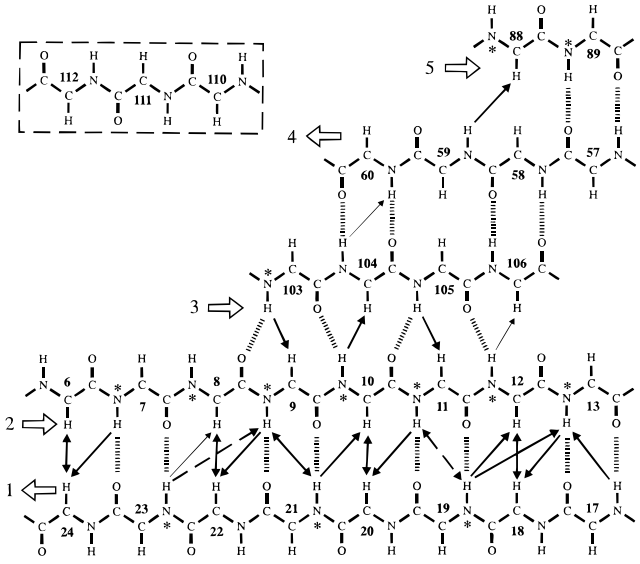

FIGURE 5: Sheet structure of oxidized and reduced human ferredoxin deduced from NOE data. Solid arrows (thick line) indicate interstrand NOEs detected for both oxidation states. Solid arrows (thin line) indicate interstrand NOEs detected only for oxidized state. Broken line arrows indicate interstrand NOEs detected only in the reduced state. Strands 4 and 5 are shown as described for putidaredoxin (*25*), consistent with the limited set of unambiguous interstrand NOEs observed in human ferredoxin. The box of broken lines shows the extra strand indicated by CSI for the reduced HuFd. Dotted lines represent putative hydrogen bonds. Slowly exchanging amide protons for oxidized HuFd are indicated with asterisks.

showed similar patterns of shift degeneracy and line broadening in both oxidation states. An NOE linking strands 3 and 4 was observed only in spectra of the oxidized protein, but an NOE was observed in both oxidation states of HuFd linking residues in strands 4 and 5 of the β-sheet structure analogous to that reported for putidaredoxin (Figure 5). Overlap of the H^{N} resonances of Thr^{104} (8.74) and Glu^{60} (9.10

ppm) and the intense signals of the diagonal may account for the failure to observe any cross-strand NOEs in the reduced protein.

Qualitative hydrogen exchange rates were determined from 2D ^{1}H[^{15}N] HSQC spectra of a sample of oxidized [U-^{15}N]-HuFd dissolved in ^2H_2O. Those residues whose backbone amide protons show slow exchange are indicated by asterisks in Figure 4A. Residues with slow hydrogen exchange rates occur in regions of identified secondary structure. Hydrogen exchange rates were not determined for reduced HuFd.

DISCUSSION

Assignments. Human ferredoxin proved to be a more challenging protein for NMR study than other [2Fe-2S] ferredoxins we have studied, owing to its different paramagnetic properties and lower stability. The hyperfine-shifted resonances of human ferredoxin have much shorter T_1 values and broader line widths (B. Xia and J. L. Markley, unpublished results) than those of the *Anabaena* 7120 vegetative (*28*) and heterocyst (*29*) ferredoxins. Assignments were made for ~70% of the residues of oxidized HuFd and ~80% of reduced HuFd. With the exception of the C-terminal 10 residues in oxidized HuFd, those residues whose signals were not observed in 3D data sets are expected to be ligated to, H-bonded to, or close in space to the cluster. In the case of the *Anabaena* 7120 vegetative ferredoxin, for which NMR data (*26*) could be compared with an X-ray structure (*30*), it was found that (^{1}H, ^{13}C) and (^{1}H, ^{15}N) cross-peaks were not observed in NMR spectra when the hydrogens were located closer than ~7 Å to one of the iron atoms.

As has been observed with other [2Fe-2S] ferredoxins (*26*), paramagnetic effects in both oxidation states made it difficult to derive extensive sequence-specific assignments from NOE data. Studies of other iron−sulfur proteins have shown the benefit of using through-bond connectivities observed by 2D (*26*) and 3D (*27*) NMR for determining assignments, and those reported here were derived primarily from 3D triple-resonance data.

Residue types could be deduced in certain cases from characteristic $^{13}C^{\alpha}$ and $^{13}C^{\beta}$ chemical shifts, and these served as starting points for sequential assignments. This approach obviated the need for selective labeling, which was used to determine starting points for sequential assignments for the *Anabaena* 7120 heterocyst ferredoxin (*27*). Although additional data sets (3D ^{15}N-TOCSY−HSQC, 3D C(CO)NH, and 3D H(CCO)NH) were collected in attempts to extend the assignment to side chains, they were of limited usefulness, and few side-chain protons beyond H^{α} or carbons beyond C^{β} were assigned.

Figure 6 shows a comparison of the assignment results for oxidized HuFd with those from three other [2Fe-2S] ferredoxins whose oxidized-state, sequence-specific NMR assignments have been determined: *Anabaena* 7120 vegetative ferredoxin (*26*), *Anabaena* 7120 heterocyst ferredoxin (*27*), and putidaredoxin (*9*). In this figure, underlined letters denote residues whose signals were observed and assigned, and those not underlined denote residues whose signals in the diamagnetic region were not observed (or only partially observed). With the exception of the C-terminal decapeptide of HuFd, the regions of unassigned residues (black) are conserved among these four [2Fe-2S] ferredoxins and are

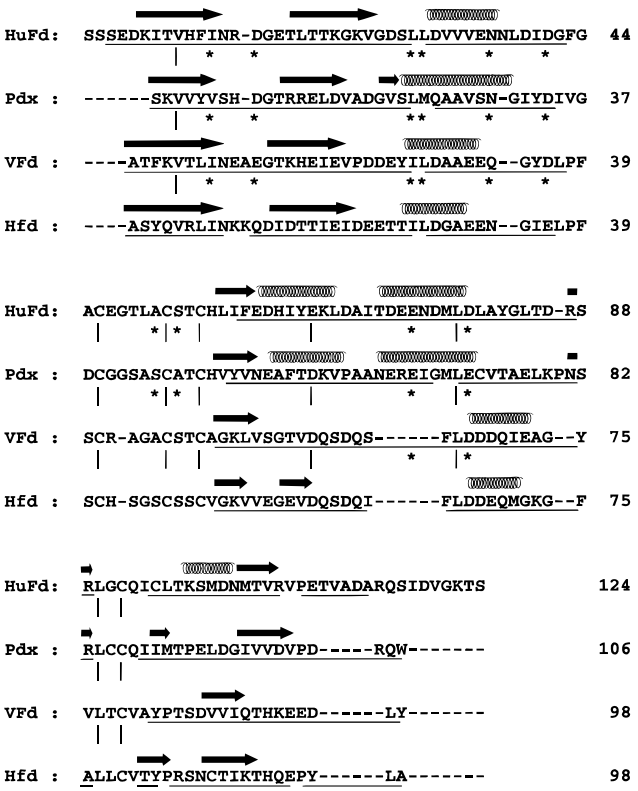

FIGURE 6: Comparison of protein sequences and oxidized state secondary structures for human ferredoxin (HuFd), putidaredoxin (Pdx) (*9*, *25*), *Anabaena* 7120 vegetative ferredoxin (VFd) (*26*, *30*), and *Anabaena* 7120 heterocyst ferredoxin (HFd) (*27*, *40*). Underlined letters denote residues whose signals were assigned by conventional diamagnetic NMR methods. The other residues were not assigned. Identical residues (|) and similar residues (*) are indicated.

located, for the most part, near the aligned ligand cysteines. In addition, paramagnetic effects appear to affect Leu^{30} in oxidized human ferredoxin and its homologous residues in other three proteins. As with the corresponding proline of *Anabaena* heterocyst ferredoxin, no assignments were made to Val^{107} and Pro^{108} in oxidized HuFd. Rather than being a paramagnetic effect, this probably is a consequence of the assignment strategy employed, which does not trace sequential assignments through proline; signals from corresponding residues of the other [2Fe-2S] ferredoxins were assigned.

It is postulated here that exchange effects, rather than paramagnetic effects, prevented the observation of signals from the C-terminal 10 residues in the 3D NMR spectra. The rationale behind this assumption is that a previous NMR study of bovine adrenodoxin indicated that the C-terminal part of the protein rotates freely in solution (*31*) and that a mutagenesis study showed that the C-terminal 14 residues of bovine adrenodoxin, which correspond to the C-terminal 10 residues of HuFd, are not essential for protein function (*32*). The exchange broadening effects in this region could be a consequence of structural disorder that results in exchange effects on an intermediate time scale for the chemical shift (lifetimes of microseconds to milliseconds) as can arise from exchange of solvent-exposed backbone amide hydrogens or internal motions.

No signals were observed for Ser^1 or Ser^2 in either oxidation state. As with the C-terminus, the reason for this may be exchange broadening.

As with other [2Fe-2S] ferredoxins, signals from residues in the two stretches that include the cluster ligands, Gly^{44}−Leu^{57} and Leu^{90}−Ile^{94}, did not appear in the 3D spectra of oxidized or reduced HuFd. Elsewhere in the molecule, oxidation-state-dependent differences were seen in the patterns of nonobserved residues. In spectra of reduced HuFd, signals were assigned to Leu^{30} but not to Leu^{29}; conversely, for oxidized HuFd, signals were assigned to Leu^{29} but not to Leu^{30}. Whereas signals were assigned to Arg^{106} in oxidized HuFd, no signals were assigned to the stretch including this residue Arg^{106}−Pro^{108} in the reduced protein. Signals from Met^{77} and Leu^{78} were missing only in spectra of the reduced protein. The residues in putidaredoxin homologous to these latter two residues (Met^{70} and Leu^{71}) were reported to be affected by paramagnetism (*9*). The presence of signals from Ala^{114} in oxidized HuFd, but their absence in the reduced protein, suggests that this residue is affected differentially by the paramagnetism of the [2Fe-2S] cluster in the two oxidation states.

Secondary Structure. Independent information on the secondary structure of oxidized HuFd was obtained from the chemical shift index (Figure 3), the pattern of NOE cross-peaks (Figure 4), and the pattern of hydrogen exchange rates (Figure 4). The results from these three different types of data were in partial agreement, as noted above for the lengths of helices and strands. Most significantly, β-strands 4 and 5 were not predicted by the CSI in either the oxidized or reduced protein. This suggests that the CSI, which has proved to be a reliable indicator for secondary structure in diamagnetic proteins, must be interpreted with caution when used with paramagnetic proteins, especially for residues adjacent to those affected by paramagnetic broadening.

CSI analysis (Figure 3) failed to predict the first helix for reduced HuFd suggested by NOE data (Figure 4). CSI analysis predicted that helix A in oxidized HuFd consists of residues 31−35, but predicted no helix for this stretch in the reduced protein, despite the fact that the chemical shifts of residues 33−35 are almost identical in the two oxidation states. By contrast, the NOE data indicated the presence of a somewhat longer helix A (31−37) in oxidized HuFd and a shorter helix A (34−37) in the reduced state.

The third strand predicted by CSI for oxidized HuFd ferredoxin (104−106) was not predicted by the CSI plot for reduced HuFd, largely because chemical shifts for residue 106 were not determined for the latter. Strands 4 and 5 which were not predicted by the CSI in either oxidation state are similarly affected by proximity to the cluster. On the other hand, the NOE data suggest that residues 103−105 of reduced HuFd form a strand; this strand probably also is present in the reduced state because the chemical shifts of nuclei in residues 104 and 105 are similar in the two oxidation states.

CSI analysis predicted that residues 72−79 form a helix in both oxidation states. NOE data confirmed this for oxidized HuFd, but no NOEs were observed for residues 77 and 78 of reduced HuFd. However, the chemical shifts of the $^{13}C^{\alpha}$ and $^{13}C^{\beta}$ of residue 78 in reduced HuFd (obtained from the CBCA(CO)NH experiment) are almost identical to those in oxidized HuFd. This is consistent with helix C in reduced HuFd extending to residue 79 as in oxidized HuFd.

The β-sheet topology reported for putidaredoxin by Ye and Pochapsky (*25*) is consistent with the NOEs observed for HuFd (Figure 5). The evidence from HuFd data for the existence and positioning of strands 4 and 5 is relatively weak, however. In HuFd, a combination of chemical shift degeneracy (e.g., Phe^{59} $H^{\alpha} = 4.56$ ppm, Val^{105} $H^{\alpha} = 4.62$ ppm) and paramagnetic broadening (residues 57, 58, 89, 106, and 107) may account for the lack of additional unambiguous cross-strand NOEs linking β-strands 3/4 and 4/5.

The CSI results for reduced HuFd predict that residues 110−112 form a β-strand (Figure 3). However, the lack of unambiguous cross-strand NOEs to this stretch prevented our determination of where it should be positioned in the overall protein structure (Figure 5).

Structural Differences between Oxidized and Reduced Human Ferredoxin. Probably the clearest evidence for a structural difference between the oxidized and reduced form of the protein comes from changes in the C-terminus. The fact that 3D NMR signals from the last 10 residues were observed and assigned in reduced HuFd but not in the oxidized form suggests that this region is more structured when HuFd is reduced than when it is oxidized.

Additional evidence may come from chemical shift differences between the two states. However, care must be exercised in interpreting such changes with a paramagnetic protein such as HuFd, because residues affected by the paramagnetism will experience oxidation-state-dependent chemical shift changes in the absence of a conformational change. Thus such shift changes can be ascribed to a conformational change only if they do not arise from contact or pseudocontact interactions with unpaired electron density. It may be anticipated that signals affected by the paramagnetism of the [2Fe-2S] cluster would be broadened to the extent that they would not be observed in multidimensional NMR spectra, but this is an assumption that needs to be examined closely.

Oxidation-state-dependent structure changes have been proposed, nevertheless, for bovine adrenodoxin on the basis of changes in $^{1}H^{\alpha}$ and $^{1}H^{\beta}$ chemical shifts (*33*). In this study, signals were assigned to fewer than 20% of the residues, and few oxidation-state-dependent shift were reported for residues 29−32 or 109−114. Large chemical shift differences were observed in adrenodoxin for Ala^{81} and Tyr^{82} (*33*). However, the $^{1}H^{\alpha}$ resonances of the corresponding residues in HuFd (Ala^{81} and Tyr^{82}) each showed oxidation-state-dependent shift differences of only about 0.2 ppm. In HuFd, $^{1}H^{\alpha}$ shift differences of this magnitude and larger were observed for residues in stretches 27−30 and 109−114: e.g., 0.54 ppm for Asp^{27}, 0.30 ppm for Leu^{29}, and 0.65 for Val^{111}. A similar pattern was seen for ^{13}C chemical shift differences in HuFd (Figure 7): those for Ala^{81} and Tyr^{82} are smaller than those for residues 29−32 and 109−114.

The fact that the largest chemical shift differences observed in the diamagnetic region of the ^{13}C NMR spectrum are seen in regions well separated from the cluster ligands, and also adjacent to the C-terminal region for which NMR evidence indicates an oxidation-state-dependent change in structural stability, lends credence to the idea that they may arise from bona fide conformational differences. Thus, the pattern of chemical shift perturbations in HuFd is consistent with the largest oxidation-state-dependent structural changes occurring around residues 29−32 and 109−114; smaller changes may

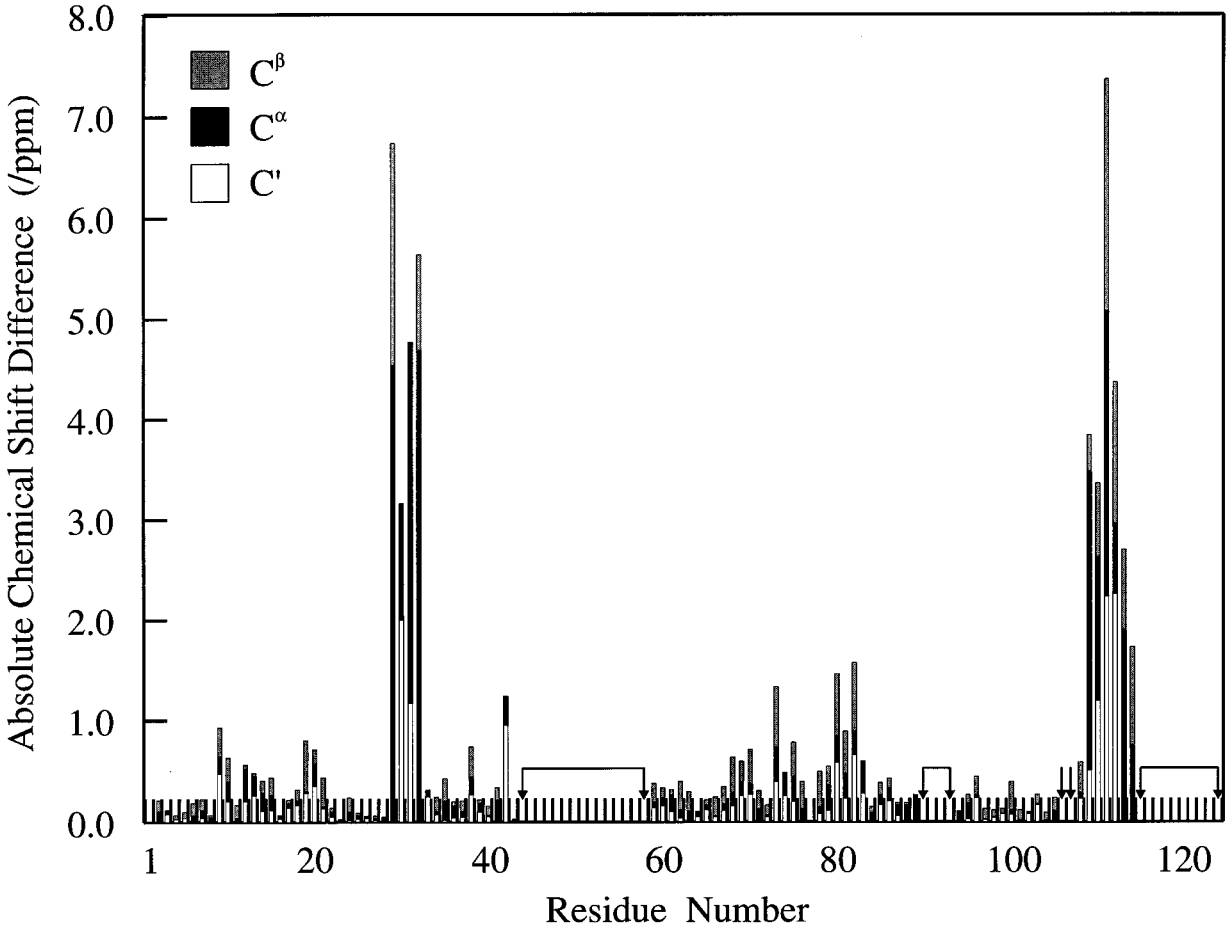

FIGURE 7: $^{13}C'$, $^{13}C^{\alpha}$, and $^{13}C^{\beta}$ chemical shift differences between oxidized and reduced human ferredoxin. Arrows indicate residues whose chemical shifts were not determined in either oxidized or reduced states.

occur in the vicinity of residues 81−82, as suggested for adrenodoxin (*33*).

The NMR data indicate possible oxidation-state-dependent changes in secondary structure. The observation of large chemical shift differences for residues 31−32 is consistent with the shortening of helix A in reduced HuFd deduced from NOE data. Signals from residue 30 of oxidized HuFd were not observed, whereas signals from residue 29 of reduced HuFd were not observed. This may indicate that Leu[29] is closer to the [2Fe-2S] cluster in the reduced state, whereas Leu[30] is closer to the cluster in the oxidized state. Thus, reduction of the cluster probably leads to loss of helix at residues 31−33 and repositioning of residues 29 and 32.

Structural Implications. In the biological process of cholesterol side-chain cleavage, reduced ferredoxin reductase binds to oxidized human ferredoxin, reduces it, and then releases it. Next, the reduced human ferredoxin binds to oxidized cytochrome $P450_{scc}$ and transfers the electron to it. Our present results suggest that oxidized HuFd undergoes a structural transition upon reduction that changes the structure of the C-terminal residues. A previous study demonstrated that deletion of C-terminal residues 116−128 of bovine adrenodoxin led to no change in its affinity for ferredoxin reductase, but caused a 1.5-fold higher affinity for cytochrome $P450_{scc}$ and enhanced activity for the cholesterol side-chain cleavage reaction (*32*). A recent study also showed that a mutant of bovine adrenodoxin with more residues deleted (*des* 109−128) had higher affinity for cytochrome $P450_{scc}$ than one with fewer residues deleted (*des* 115−128) (*34*). These results suggest that the C-terminal residues interfere with binding to cytochrome $P450_{scc}$. Therefore, we hypothesize that ferredoxin reductase binds preferentially to oxidized HuFd (the state with the flexible C-terminus) and that reduced HuFd is released as a consequence of the conformational change in the C-terminus that accompanies its reduction. Previous studies have suggested that ferredoxin reductase binds the oxidized form of bovine ferredoxin more tightly than the reduced form (*35*) and that the two forms compete for the same binding site (*36*).

A mutant of adrenodoxin lacking residues 108−128 was found not to form an iron−sulfur cluster in vivo when expressed in *E. coli*, whereas the truncated version that is one residue longer (*des* 109−128) does form the cluster (*34*). A subsequent study showed that a [2Fe-2S] cluster can be inserted into *des* 108−128 adrenodoxin by in vitro reconstitution. The two truncated adrenodoxins were found to have similar spectroscopic, functional, and redox properties, but that lacking Pro[108] had a lower stability (*37*). It was suggested on this basis that Pro[108] may play a role in stabilizing the cluster. However, the present results show that the chemical shifts and line widths of the $^{13}C'$, $^{13}C^{\alpha}$, $^{13}C^{\beta}$, and $^{1}H^{\alpha}$ of Pro[108] of HuFd are quite similar in both oxidation states; this appears to rule out a direct interaction of this residue with the cluster. On the other hand, Val[107] in oxidized HuFd and Arg[106] and Val[107] in reduced HuFd were not identified in the 3D triple-resonance spectra. These line broadening effects (manifested as missing signals in 3D spectra) suggest that residues 106 and 107 may interact with

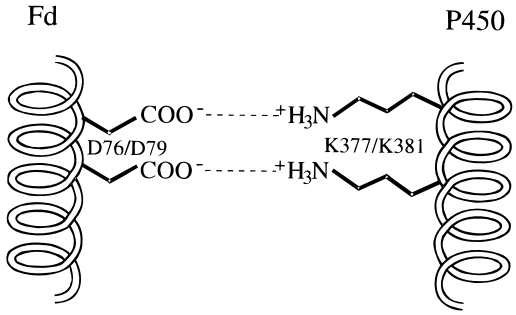

FIGURE 8: Speculative model indicating the role of charged residues in the binding interaction between ferredoxin (Fd) and cytochrome $P450_{scc}$ (P450).

the iron−sulfur cluster. The deletion of Pro^{108} may destabilize protein by indirect interactions with these adjacent residues.

Asp^{76} and Asp^{79} have been shown to be critical for the binding of human ferredoxin to NADPH-dependent ferredoxin reductase and to cytochrome $P450_{scc}$ (*38*). Substitutions of other amino acids at these two positions cause striking decreases in activity and in the affinity of HuFd for both ferredoxin reductase and cytochrome $P450_{scc}$. The present results reveal that Asp^{76} and Asp^{79} are located in an α-helix. Because they play an important role in binding the ferredoxin reductase and cytochrome $P450_{scc}$, these two residues must be positioned at the outer side of the helix so that their side chains are accessible to the solvent. Sequential connectivities were not observed for Met^{77} and Leu^{78} of reduced HuFd. Thus, these two residues likely are affected by the iron−sulfur cluster and must be relocated closer to the iron−sulfur cluster binding pocket when HuFd is reduced. Site-directed mutagenesis studies have shown that two lysine residues of cytochrome $P450_{scc}$, Lys^{377} and Lys^{381}, are crucial for binding adrenodoxin (*39*). We suggest that Asp^{76} and Asp^{79} of human ferredoxin may interact with Lys^{377} and Lys^{381} of cytochrome $P450_{scc}$ through charge−charge interactions. Considering the fact that the two aspartate residues are located within a helix and separated by about one turn of the helix, the two lysine residues, which share a similar spacing, also may be located within a helix of cytochrome $P450_{scc}$ (Figure 8).

ACKNOWLEDGMENT

The authors thank Dr. Frits Abildgaard for help in setting up some NMR experiments, Dr. John Olson for assistance in using CONTRAST software, Dr. Roger Chylla for help in using PEAKPICK software, and Dr. Larry E. Vickery for stimulating discussions.

REFERENCES

1. Mittal, S., Zhu, Y., and Vickery, L. E. (1988) *Arch. Biochem. Biophys. 264*, 383−391.
2. Xia, B., Cheng, H., Skjeldahl, L., Coghlan, V. M., Vickery, L. E., and Markley, J. L. (1995) *Biochemistry 34*, 180−187.
3. Mason, J. I., and Boyd, G. S. (1971) *Eur. J. Biochem. 21*, 308−321.
4. Simpson, E. R., and Miller, D. A. (1978) *Arch. Biochem. Biophys. 190*, 800−808.
5. Suhara, K., Takemori, S., and Katagiri, M. (1972) *Biochim. Biophys. Acta 263*, 272−278.
6. Marg, A., Kuban, R.-J., Behlke, J., Dettmer, R., and Ruckpaul, K. (1992) *J. Mol. Biol. 227*, 945−947.
7. Greenfield, N. J., Wu, X., and Jordan, F. (1989) *Biochim. Biophys. Acta 995*, 246−254.
8. Miura, S., Tomita, S., and Ichikawa, Y. (1991) *J. Biol. Chem. 266*, 19212−19216.
9. Pochapsky, T. C., Ye, X. M., Ratnaswamy, G., and Lyons, T. A. (1994) *Biochemistry 33*, 6424−6432.
10. Lambeth, J. D., Saybert, D. W., Lancaster, J. R., Jr., Salerno, J. C., and Kamin, H. (1982) *Mol. Cell. Biochem. 45*, 13−31.
11. Usanov, S. A., Chashchin, V. L., and Akhrem, A. A. (1997) *Front. Biotransform. 3*, 1−57.
12. Xia, B., Cheng, H., Bandarian, V., Reed, G. H., and Markley, J. L. (1996) *Biochemistry 35*, 9488−9495.
13. Coghlan, V. M., and Vickery, L. E. (1989) *Proc. Natl. Acad. Sci. U.S.A. 86*, 835−839.
14. Huang, J. J., and Kimura, T. (1973) *Biochemistry 12*, 406−409.
15. Kay, L. E., Xu, G. Y., and Yamazaki, T. (1994) *J. Magn. Reson. A 109*, 129−133.
16. Grzesiek, S., and Bax, A. (1992) *J. Magn. Reson. 96*, 432−440.
17. Wishart, D. S., Bigam, C. G., Yao, J., Abildgaard, F., Dyson, H. J., Oldfield, E., Markley, J. L., and Sykes, B. D. (1995) *J. Biomol. NMR 6*, 135−140.
18. Edison, A. S., Abildgaard, F., Westler, W. M., Mooberry, E. S., and Markley, J. L. (1994) *Methods Enzymol. 239*, 3−79.
19. Chylla, R. A., and Markley, J. L. (1993) *J. Magn. Reson. B 102*, 148−154.
20. Olson, J. B., Jr., and Markley, J. L. (1994) *J. Biomol. NMR 4*, 385−410.
21. Olson, J. B., Jr. (1995) Ph.D. Thesis, University of Wisconsin−Madison, Madison, WI.
22. Wishart, D. S., and Sykes, B. D. (1994) *J. Biomol. NMR 4*, 171−180.
23. Wishart, D. S., and Sykes, B. D. (1994) *Methods Enzymol. 239*, 363−394.
24. Wüthrich, K. (1986) *NMR of Proteins and Nucleic Acids*, Wiley, New York.
25. Ye, X. M., and Pochapsky, T. C. (1992) *Biochemistry 31*, 1961−1968.
26. Oh, B.-H., and Markley, J. L. (1990) *Biochemistry 29*, 3993−4004.
27. Chae, Y. K., Abildgaard, F., Mooberry, E. S., and Markley, J. L. (1994) *Biochemistry 33*, 3287−3295.
28. Cheng, H., Westler, W. M., Xia, B., Oh, B.-H., and Markley, J. L. (1995) *Arch. Biochem. Biophys. 316*, 619−634.
29. Chae, Y. K., and Markley, J. L. (1995) *Biochemistry 34*, 188−193.
30. Rypniewski, W. R., Breiter, D. R., Benning, M. M., Wesenberg, G., Oh, B.-H., Markley, J. L., Rayment, I., and Holden, H. M. (1991) *Biochemistry 30*, 4126−4131.
31. Miura, S., and Ichikawa, Y. (1991) *Eur. J. Biochem. 197*, 747−757.
32. Cupp, J. R., and Vickery, L. E. (1991) *J. Biol. Chem. 263*, 17418−17421.
33. Miura, S., and Ichikawa, Y. (1991) *J. Biol. Chem. 266*, 6252−6258.
34. Uhlmann, H., Kraft, R., and Bernhardt, R. (1994) *J. Biol. Chem. 269*, 22557−22564.
35. Lambeth, J. D., McCarslin, D. R., and Kamin, H. (1976) *J. Biol. Chem. 251*, 7545−7559.
36. Hanikoglu, I., and Jefcoate, C. R. (1980) *J. Biol. Chem. 255*, 3057−3061.
37. Uhlmann, H., Iametti, S., Vecchio, G., Bonomi, F., and Bernhardt, R. (1997) *Eur. J. Biochem. 248*, 897−902.
38. Coghlan, V. M., and Vickery, L. E. (1991) *J. Biol. Chem. 266*, 18606−18612.
39. Wada, A., and Waterman, M. R. (1992) *J. Biol. Chem. 267*, 22877−22882.
40. Jacobson, B. L., Chae, Y. K., Markley, J. L., Rayment, I., and Holden, H. M. (1993) *Biochemistry 32*, 6788−6793.

BI972722H